*Journal of Machine Engineering, 2019, Vol. 19, No. 3, 94–107*
*ISSN 1895-7595 (Print) ISSN 2391-8071 (Online)*

Received: *08 February 2019* / Accepted: *12 June 2019* / Published online: *25 September 2019*

*additive manufacturing, steel, implicit/explicit, thermal cycles*

Johannes BUHL[1*]
Rameez ISRAR[1]
Markus BAMBACH[1]

# MODELING AND CONVERGENCE ANALYSIS OF DIRECTED ENERGY DEPOSITION SIMULATIONS WITH HYBRID IMPLICIT / EXPLICIT AND IMPLICIT SOLUTIONS

Conventional metal manufacturing techniques are suitable for mass production. However, cheaper and faster alternatives are preferred for small batch sizes and individualized components. Directed energy deposition (DED) processes allow depositing metallic material in almost arbitrary shapes. They are characterized by cyclic heat input, hence heating and cooling every point in the workpiece several times. This temperature history leads to distribution of mechanical properties, distortions, residual stresses or even fatigue properties in the part. To avoid experimental trial-and-error optimization, different methods are available to simulate DED processes. Currently, the wire arc additive manufacturing (WAAM) is the most competitive DED process. In this work, a simulation method for the WAAM process is established and validated, which should be capable to calculate global effects (e.g. distortions, residual stresses) of real WAAM-processes with duration of hours and thousands of weld beads. The addition of beads and layers is simulated by the element birth and death technique. The elements are activated according to the movements of the heat source (arc). In this paper, the influence of the time step, the mesh size and the material properties of the inactive elements in hybrid implicit / explicit and fully implicit solutions are evaluated with respect to the computation time and stability. This investigation concludes several recommendations for AM-modelling. For example, a low Young's modulus (100 N/mm²) for the inactive elements show nearly no influences on the welding simulation, but introduces numerical instabilities in case of multiple welding beads. The Young's modulus should be increased to 1.000 N/mm² for small mesh-sizes, small step-sizes and many beads, even when it introduces unwanted stresses.

## 1. SIMULATION POSSIBILITIES FOR ADDITIVE MANUFACTURING

### 1.1. ADDITIVE MANUFACTURING

Traditional manufacturing processes are suitable for mass production. However, for small batch sizes and individualized components, the manufacturing cost increases due to the inevitable tooling costs. Additive manufacturing (AM) requires no tooling and is more suitable for customized and complex parts. Currently, directed energy deposition (DED),

[1] Brandenburg University of Technology Cottbus–Senftenberg, Dept. of Mechanical Design and Manufacturing, Cottbus, Germany
[*] E-mail: johannes.buhl@b-tu.de
https://doi.org/10.5604/01.3001.0013.4086

especially wire-arc additive manufacturing (WAAM), is considered as one of the most competitive 3D printing technologies for medium to large-scale parts [1]. The wire-arc process builds up the required shape by successive layer-by-layer depositing. However, the path strategy, the deposition rate, the cooling and clamping of the part influence the local part properties and the obtained geometry. Due the long processing times of the WAAM-process, an experimental trial-and-error optimization is comparatively difficult, time consuming and cost-intensive. Especially for time-dependent processes, numerical simulations are highly useful to predict and optimize the process.

### 1.2. SIMULATION METHODS FOR DED

The simulation proposed for DED can be categorized according to the meshing strategies in relation with the physical principles being modelled. The individual beads of the AM-part are designed by meshed and non-meshed simulation methods [2]. Meshed simulation methods usually have elements that are connected to each other e.g. Lagrangian method [3], Eulerian method [4], Arbitrary Lagrangian-Eulerian (ALE) method [5], Computational Fluid Dynamics (CFD) [6], or the Conservation Element and Solution Element (CESE) method [7]. On the other hand, the meshless simulation methods uses particles to simulate different mechanical behaviours, for example Discrete Element Method (DEM) [8], Smoothed Particle Hydrodynamics [9] and Element Free Galerkin (EFG) method [10].

The mesh based simulation methods offer many advantages. For example, the Lagrangian method is very useful for the solution of computational solid mechanics problems where the deformations are conditioned. This method is very efficient for thermo-mechanical and forming problems and it saves computational time. The Eulerian method was established for applications with large deformations and flow-simulations of fluids.

Almost all hydrodynamics problems can be solved with the Eulerian method, and it calculates the mass, energy and momentum conservation efficiently [2]. ALE simulation combines the advantages of Lagrangian and Eulerian simulation methods and can be utilized in problems where large deformations take place and material flow tracking is important. A good aspect ratio of the elements can be preserved in this method using methods like mesh update or remeshing techniques [11].

CESE method is very effective in transient flow simulation where high numerical accuracy is required. This method efficiently controls numerical dissipation [12] and is used for discontinuous flow problems i.e. shock waves, acoustic waves, chemical reaction and cavitation [7]. CFD has been found suitable for compressible and non-compressible fluids. It provides solution to various problems like heat transfer, turbulence, fluid flow and combustion reactions [13].

Meshless simulation methods usually deal with the processes where high deformation takes place. Therefore, the Element Free Galerkin (EFG) method is computationally time efficient because element distortions cannot take place [14]. SPH is quite capable of simulating processes like forming, fusion, phase change, wave flow [15], complex fluid interactions and fracture [16, 17]. DEM is reliable at estimating forces between particles [18]

and their collision behaviour in relation to external conditions [19]. SPH can be used to simulate details of an arc welding process such as the physical effects of drop formation, solidification of the material and the development of pores, while respecting the geometry of the weld bead.

The use of a particular simulation method depends highly on the process requirements and the expected outcomes. In this work, a simulation method for WAAM is established, which can be used for a real part where thousands of beads form a part. A further requirement on the simulation method is the ability to calculate processes in the range of hours without time scaling. A meshed Lagrangian simulation method is used, in which the material properties can be activated with the deposition torch.

### 1.3. LAGRANGIAN METHOD WITH EXPLICIT-IMPLICIT SOLVERS

Implicit and explicit methods are used to solve the finite element equations [20]. The implicit method uses an iterative scheme until the required convergence criteria is satisfied and equilibrium is reached [20]. This method is promising if the deformations or the thermal changes in the model are less in one time step. Time steps in which multiple contacts occur or in which a high deformation must be solved cause instabilities and it is difficult to attain the equilibrium. The equilibrium and divergence should be controlled during the calculation [21, 22]. Many iterations in a time step increase the total calculation time [23, 21]. The solidification process for thermo-mechanical models mostly use implicit simulation method [24]. If the solver is controlled with a proper automatic time step adjustment, the calculations with a high accuracy become extremely fast.

The explicit method does not use iterations. That makes the simulation routine robust and the computational costs are linearly proportional to the size of the model [20]. If the time step size is smaller than a critical time (i.e. dilatational wave is required to cross any element in the mesh) the explicit method is stable even for analysis with a high dynamic [21, 23]. A very small time step is advantageous for stability of contact, the explicit method is usually used to simulate processes with a short time [22, 25]. In case of large computational problems the inertia and dynamic effects becomes high, which reduces the accuracy of the solution [23].

In order to reduce the computational time in explicit calculations, the mass of the elements are increased by maintaining the accuracy of the solution [23]. The mass is usually scaled by increasing the material density [22]. Therefore, a proper and suitable scaling factor must be chosen carefully while using the explicit method. [23].

### 1.4. HYBRID EXPLICIT/IMPLICIT CODE FOR LAGRANGIAN WELDING-MODELS

Perhaps the first finite element analysis on thermal elastic-plastic stress and strain during a welding process was published in 1970 in Japan. Computational Welding Mechanics (CWM) is concerned with the thermo-mechanical response as well as changes in microstructure [26]. Implicit calculation methods with high computation times, can be speed

up with iterative substructure methods as shown in [27]. Compared to the implicit method, dynamic thermo-mechanical analysis with a short process time can be solved in a short time using an explicit solver. The following Table 1 gives a brief evaluation of both methods for large deformation, dynamic effects, large process time, computation time, possibilities for speed up, price of hardware. It can be seen, that the dynamic implicit solver features convincing properties for CWM-simulations.

Table 1. Comparison of implicit and explicit solver

| | Explicit | Implicit static (dynamic) | References |
|---|---|---|---|
| Large deformation | ++ | – – (+) | [20, 23, 24 |
| Dynamic effects | ++ | – – (+) | [20, 21, 23, 25] |
| Large process time | – – | + (++) | [20, 21, 23] |
| Computation time | + | ++ (++) | [20, 23, 25] |
| Possibilities for speed up | ++ | – – (– –) | [20, 23, 24, 25] |
| Price of hardware | ++ | – – (– –) | - |

Nowadays, dynamic thermo-mechanical analysis are often divided whereby the thermal part is computed implicitly and mechanical part explicitly [20] [23]. Another possibility to save computation time is to solve the welding with the hybrid method and the cooling is done completely implicitly [28].

To find a fast and stable method for AM-simulations of entire parts, there are many possibilities to couple and uncouple the thermal and mechanical calculations, as well as explicit and implicit solver. The effect of using coupled and uncoupled, pure and hybrid solvers on the computation time, cost, time step and mesh size has not been shown for multiple beads, which are joined together or even complete DED processes. Similarly, ghost material has been used for welding simulations [32, 33], but its influence on the accuracy and stability of multiple welding beads or real WAAM-simulation is unknown.

### 1.5. AIM OF THIS RESEARCH

In this investigation, two finite element simulation methods are compared for a small part manufactured by AM. A fully coupled pure implicit and hybrid (implicit/explicit) method is compared to an uncoupled pure and hybrid method for simulation time, stability and accuracy. Besides the solver-configuration, a recommendation for AM-modelling is made for the mesh type and size, as well as for of the activation process.

## 2. NUMERICAL MODELLING OF DED BY WAAM

### 2.1. MATERIAL, HEAT SOURCE AND ACTIVATION PROCESS

In reference to a previous work [29], the properties of the temperature dependent material (steel grade 309-L) is used. The Young’s modulus decreases with increasing

temperature and becomes almost zero at the melting temperature. Similarly, the yield stress and the hardening modulus decrease with increasing temperature. On the other hand, the Poisson's ratio increases with temperature. Convection and radiation increase at higher temperatures because of more temperature difference with the surrounding air [30, 31].

In the inactive state, the material property has a very low Poisson's ratio, Young´s modulus and thermal expansion. The thermal properties are characterised by a high heat capacity which will be optimized and discussed later. The parameters for the distribution of heat, used in this work are taken from the previous work [29] are given in Table 2. The welding process is done with a constant power of 1840 W and a torch speed of 7.5 mm/s.

Table 2. Goldak's ellipsoidal heat source parameters [29]

| | | |
|---|---|---|
| Weld pool width | $a$ | 2.25 mm |
| Weld pool depth | $b$ | 1.6 mm |
| Forward weld pool | $c_f$ | 2.5 mm |
| Rearward weld pool | $c_r$ | 5.0 mm |
| Forward heat factor | $f_f$ | 1.0 |
| Rearward heat factor | $f_r$ | 1.0 |
| Exponent constant | $n$ | 1.0 |
| Welding voltage | $U$ | 23 Vt |
| Welding current | $I$ | 80 A |
| Weld pool energy | $Q$ | 1.84E6 mW |
| Heat source velocity | $v$ | 7.5 mm/s |

### 2.2. SIMULATION OF MATERIAL ADDITION BY ACTIVATING A GHOST MATERIAL

Deposition of the material was simulated using an element birth/activation technique, in which all the elements of the finished part are inactivate at first. Fig. 2 shows a summary of the activation of beads out of a quiet or ghost state. The Goldak's weld source [29] heats the inactive elements and activates them thermally within the temperature range of 1200°C–1210°C. To switch on the structural properties, the melting temperature in the range of 1400°C–1450°C must be reached, which are described with a thermo-elastic-plastic model *MAT_CWM 270 based on Von-Mises yield criteria and kinematic hardening law. Activated and deactivated elements can be deformed in the structure, but deactivated elements are nearly without mechanical properties. The mechanical contact between the inactive and active elements remains tied over the process time, while the thermal contact, which is time dependent, is enabled between the parts at predefined time periods. The boundary conditions for convection and radiation are coupled with the thermal contact definition. With the activation of the thermal contact, convection and radiation in the surrounding area are established, but between the two surfaces of beads only conduction takes place. More details about the activation procedure and it´s simplifications can be found in [29] for the steel grade 309-L.

In summary, the following points can be noted:

- The time-dependent location of the heat source defines the activation and thermal history of the beads.
- The mechanical properties are activated with coupled thermal history.
- Heat, which is produced by plastic deformation, can be neglected and the mechanical calculation has more effects than the thermal calculation on the simulation results.

This leads to the conclusion that it is possible to run the thermal simulation independently followed by the mechanical simulation using the results of thermal. A fully coupled simulation is not necessary.

## 3. COMPARISON OF PURE AND HYBRID IMPLICIT METHODS

### 3.1. FULLY COUPLED AND DECOUPLED HYBRID AND PURE IMPLICIT SIMULATIONS

In general, implicit models with a highly developed control mechanism are much faster than explicit calculations without mass-scaling or time-step adjustments. In this investigation, a fully coupled thermomechanical implicit model is established and used as standard. All simulations are done with double precision (ls-dyna_smp_d_R11) in LSDYNA. The implicit analysis solution method is specified with the nonlinear BFGS updates and arc length (Crisfield with damping, see LS-DYNA manual), where the stiffness reformation is done at the start of each step. The solution control is as follows: automatic stiffness reformation limit, ILIMIT = 11 per time step, displacement convergence tolerance, DCTOL = 1E–4, energy convergence tolerance, ECTOL = 1E–2, absolute convergence tolerance, ABSTOL = 1E–11. The transient analysis is done for material properties evaluated at 8 gauss points using solid elements, whereby a symmetric direct solver with the convergence tolerance of CGTOL = 1E–4, the absolute convergence tolerance, ABSTOL = 1E–10 and a relative convergence tolerance RELTOL = 1E–6 is used.

The temperature field is provided by an implicit thermal solver, where the thermal solver is coupled with the mechanical explicit as well as implicit solver. To accelerate the explicit calculation time, the mass is scaled according a critical time step $\Delta t_e$ as shown in Equation 1 [34]. The calculation is done for the critical time step $\Delta t_e = 0.0002\ s$ based on the material properties and the minimum distance in an element $L_e$ of 1.6 mm and time step $\Delta t_e = 0.05\ s$, which is a 250 times bigger step.

$$\Delta t_e = \frac{L_e}{\sqrt{\frac{E(1-v)}{(1+v)(1-2v)\rho}}} \tag{1}$$

For basic investigations a rectangular support-plate (120 mm × 121.5 mm) with the thickness of 4 mm and beads with a rectangular cross section of 4.5 mm, 80 mm and the height of 1.6 mm are modelled with the properties of steel (see Chapter 2). In Fig. 1 the results of the explicit calculation for one layer with 6 beads and one additional bead are

compared with the implicit simulation with a time step of 0.25 s. In general, the Von Mises stress distributions are similar for the various simulations.

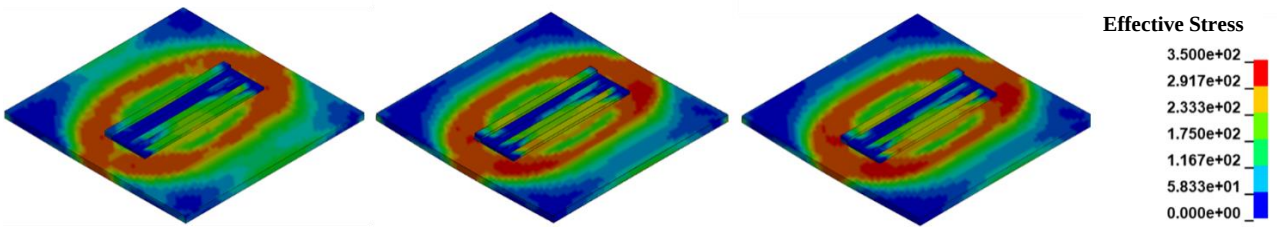


a) Explicit $\Delta t$ = 0.05 s b) Explicit $\Delta t$ = 0.0002 s c) Implicit $\Delta t$ = 0.25 s

Fig. 1. Stress-Simulation with the time step 0.05 s (a) and 0.0002 s (b) with explicit and of 0.25 s with implicit solver (c)

Differences can be seen close to the yield stress, where the heat expansion causes plastic deformation. In Fig. 2 only critical elements with an effective stress between 320 N/mm² and 375 N/mm² are shown.

(a) Explicit $\Delta t$ = 0.05 s (b) Explicit $\Delta t$ = 0.0002 s (c) Implicit $\Delta t$ = 0.25 s

Fig. 2. Elements with an effective stress of 320–375 N/mm² with the time step 0.05 s (a) and 0.0002 s (b) with explicit and of 0.25 s with implicit solver (c)

The fully coupled explicit calculation with a big time step of 0.05 s runs 53 min, for 0.0002 s 117 min and the implicit 78 min. The time-step of the thermal calculation is fixed with 0.25 s. In the fully coupled version, the explicit simulation is faster for this small task. To reduce the interaction-effort between the thermal and mechanical solver for transforming results and starting new calculation-steps, the implicit thermal calculation runs independently and the mechanical is batched. Both calculations can run simultaneously.

To reduce the interaction-effort of transforming the results and starting new calculations, the implicit thermal calculation is done with a time-step of 0.25 s for a welding time of 75 s.

Fig. 3 confirms with the temperature history, that a fully coupled simulation is not always necessary. Even the overall stress distribution shows quite similar results, a critical example is shown in Fig. 4 for the position P2 which features a more complex temperature load history. The difference in the stress between the implicit and explicit calculation increases after the welding time and confirms that the time-scaled mechanical explicit calculations are not able to build up stress relaxations. For Point P1 the welding is finished at approx. 60 s, at point P2 at 26 s, while the global cooling starts at 75 s. The big difference between the coupled and non-coupled explicit results indicates great numerical uncertainties.

Table 3. Thermal/mechanical, coupled/decoupled implicit and explicit simulations using different time steps with an Intel (R) processor i7-8700K CPU6

| Simulation | T.-impl. | M.-impl. | M.-expl. | Coupled impl. | Coupled expl. |
|---|---|---|---|---|---|
| Time step | 0.25 s | auto | 0.0002 s | 0.25 s | 0.25 s / 0.0002 s |
| Simulation time | 47 min | 11 min | 240 min | 59 min | 275 min |
| Cores | 2 | 2 | 2 | 2 | 2 |
| Memory used | 3GB | 3GB | 3GB | 3GB | 3GB |

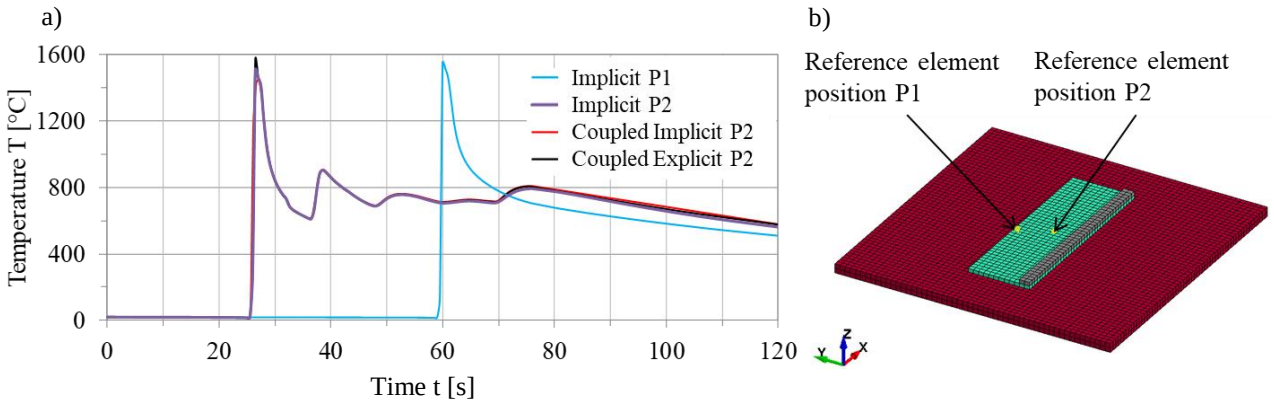


Fig. 3. Temperature distribution of standard and coupled implicit, explicit simulation (a) at two reference positions (b)

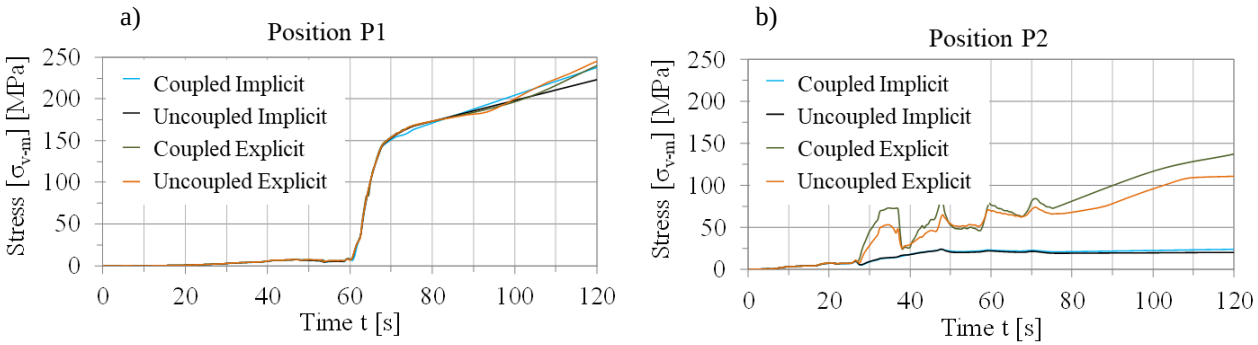


Fig. 4. Comparison of coupled and non-coupled stress distribution at position P1 (a) and position P2 (b)

It seems that the explicit simulations provide suitable results for first approaches and the complex implicit version seems convincing in details, including spring back or warpage and residual stresses after cooling.

### 3.2. AVAILABLE MESHES FOR AM-PROCESSES

Generally, many different element types are available for thermo-mechanical analyses. Often the substrate or the parts are meshed up with shell elements and the beads with solid

elements. Thin shell elements are not able the calculate shear deformation, which is highly important for shrinkage warpage, which leads to the use of solid elements in this paper.

Out of the list of hexahedra pentahedron and tetrahedron elements the linear tetrahedral and the fully integrated solid hexahedral element with poor aspect ratio and efficient formulation is used. A simple benchmark part for the AM-model is shown in Fig. 5 for a support plate having one element along the thickness with 6 beads and an additional bead on the left edge. For calculations with many thermal and mechanical cycles the hexahedral-mesh provides high stability and accuracy, while for quick estimations, tetrahedron elements could be used. So the hexahedral-mesh is recommended.

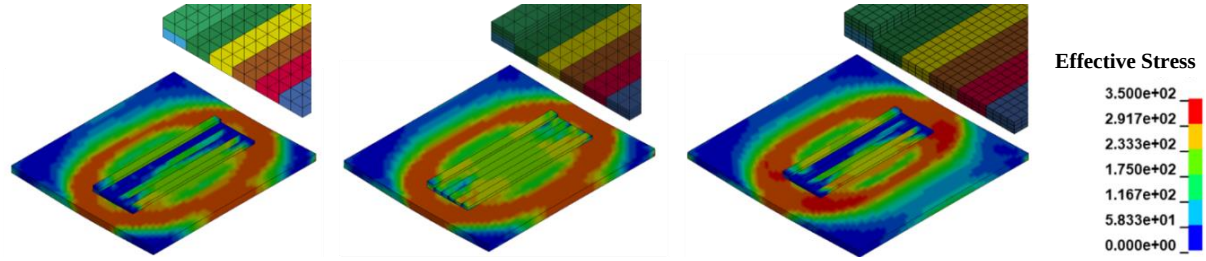


a) Tetrahedral mesh Δ*s*=1 mm b) Tetrahedral mesh Δ*s*=0.2 mm c) Hexahedral-mesh Δ*s*=0.2 mm

Fig. 5. Comparison of tetrahedral and hexahedral elements for computing the AM process

### 3.3. INFLUENCE OF STEP SIZE AND MESH-SIZE FOR IMPLICIT CALCULATIONS

Depending on the simulation aim, the cross-section of a bead can be meshed with a single element or with many elements. To see the global effects like distortion of the part or the substrate, two elements are sufficient. For residual stresses inside a bead, plastic deformation on the support a fine mesh should be used. The required mesh should have four elements in the width and three elements in the height direction (see Fig. 5c)). A reference element is selected the in the fifth layer in the middle of a bead (Fig. 6b). The step-size is adjusted in the welding process and remaining 50 s of the cooling process (Fig. 7b). Fig. 6 shows a negligible difference in the temperature development, however, the stresses calculation shows a deviation of about 10% between the rough mesh and a fine mesh with

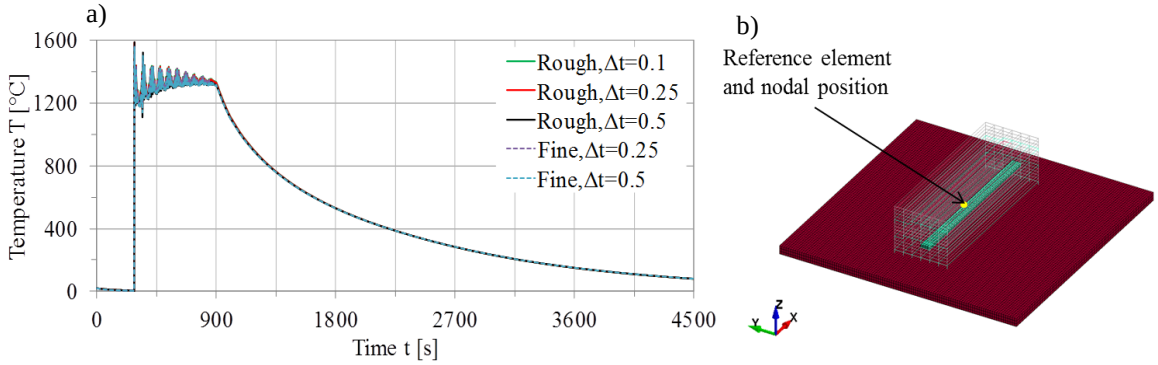


Fig. 6. Temperature history for two mesh-sizes and different time steps (a) at the referance position (b)

a step size ($\Delta t$ = 0.50 s). As the time step of rough mesh is reduced, the accuracy for stress calculation converges with the solution of the fine mesh. The maximum deviation is between the two solutions is 5%.

The effects of different time steps on the welding-simulation using a rough and fine mesh are shown in Fig. 8. A rough mesh with a time step of $\Delta t$ = 0.250 s shows equivalent results as the fine mesh with the $\Delta t$ = 0.50 s, but takes a shorter calculation time. The reason for the relative high calculation time of the rough mesh ($\Delta t$ = 0.50 s) is the high amount of iterations per step.

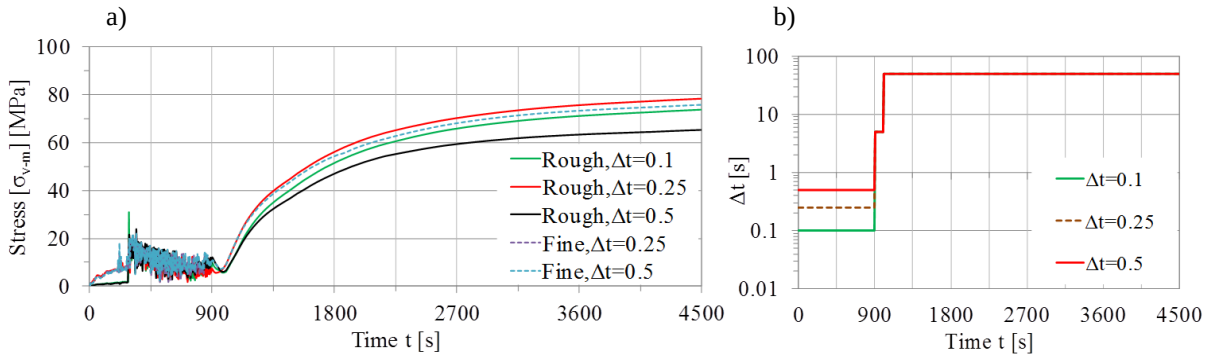


Fig. 7. History of effective stress at different time steps (a) and different timesteps used during the complete welding simulation (b)

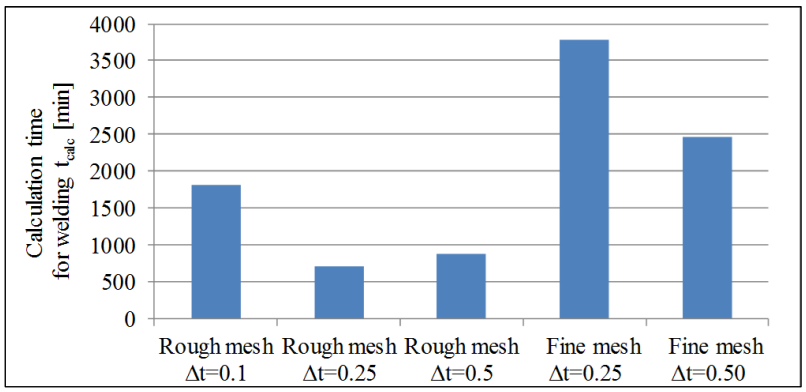


Fig. 8. Calculation time for the welding (0–900 s) for a rough and fine mesh size at different time steps with an Intel (R) processor i7-8700K CPU6

### 3.4. INFLUENCE OF GHOST PROPERTIES ON THE NUMERICAL STABILITY AND ACCURACY

The weld source heats the inactive elements and activates in order that their thermal and mechanical properties vary to simulate the adding of material. However, the material properties of the base or inactive state should be carefully chosen, so that its influence on the active elements is small. Before activation, the ghost properties are responsible not only for the numerical stability and computation time of the model, but also influence the stress-strain of the activated elements. Due to the tied contact, the inactive elements deform to according

the ghost properties. In Fig. 9 the two layers and three beads of a 14 layer box are welded (active) and all elements are visible with effective stress more than 1 N/mm². If the Young's Modulus is very small, for example $E_{Ghost}$ = 100 N/mm², the effective stress of the ghost elements does not affect the geometry of the hot beads considerably (under 1N/mm²). The disadvantage of a low Young's Modulus is a reduced numerical stability, which avoids equilibrium and cause termination of the calculation after adding 10 beads. A Young's Modulus of 1000 N/mm² shows no instability for the box (84 beads, 900 s welding time). The solver runs with double precision with high restriction for numerical accuracy (see Chapter 3). For numerical stability, the following changes require a higher Young's modulus in the Ghost state:

- Increasing total amount of time-steps;
- Higher welding time;
- Smaller mesh;
- Less numerical tolerance.

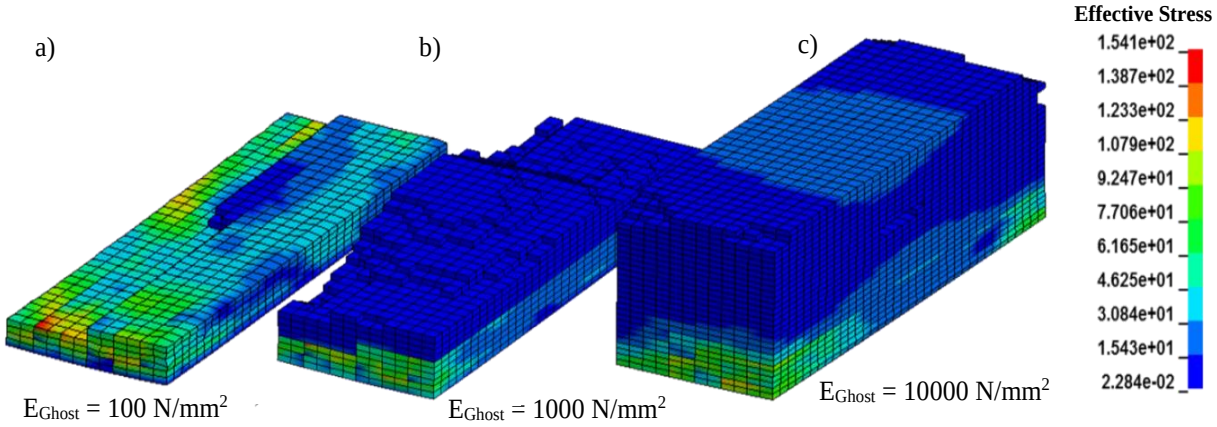


Fig. 9. Effective stress of the elements within 1 – 254 N/mm² at the time 165 s for differnet Young's modulus of the Ghost state: (a) $E_{Ghost}$ = 100 N/mm², (b) $E_{Ghost}$ = 1.000 N/mm² and (c) $E_{Ghost}$ = 10.000 N/mm² for both active and inactive elements

The thermal properties of the ghost material influence the heat flow, because the conduction is time dependent for a complete bead.

Fig. 10 shows the activation of 3 nodes in three beads adjacent to one another. The first bead has thermal contact only with the support, convection into the surrounding air and the heat source is faster than the conduction within the bead. For the second and third beads a preheating of approx. 400°C can be detected at the process-time of 10 s before the material properties are activated with the heat source at 16 s. This preheating is caused by the thermal contact activation when the welding process of the second bead starts and conduction cannot be prevented.

Fig. 10 shows the effect of different heat capacities and thermal conductivity for the ghost state compared our recommended value, which are in accordance with [29]. Because of its influence on the temperature distribution in the welded part, the thermal calibration of the model should be done after the numerical stability is reached and the ghost-properties should not be changed.

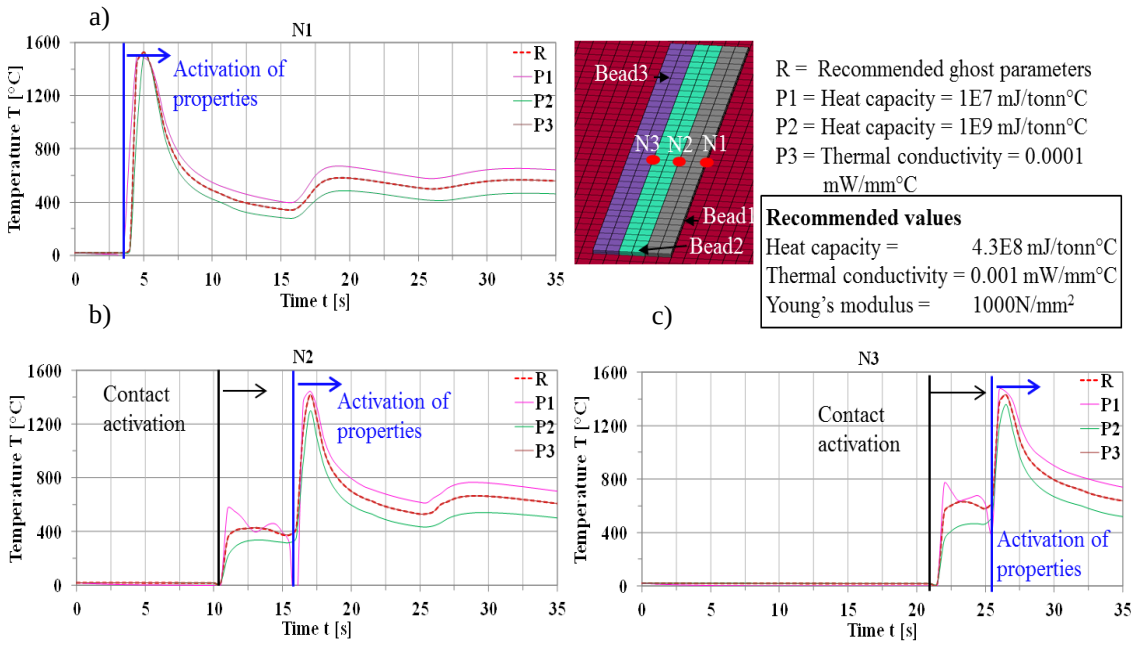


Fig. 10. History of temperature of the first (a), the second (b) and the third (c) bead for different thermal ghost properties

## 4. CONCLUSIONS AND FUTURE WORK

In this work, different simulation techniques, which are suitable to describe the WAAM-process, were investigated. The meshed Lagrangian method was selected to model the global process behaviour, which means the temperature development, the residual stresses and displacement. Using the Goldak's heat source model the local temperature was calculated to activate the ghost elements with an implicit code. Stresses and warpage were simulated with implicit and explicit solvers in a thermo-mechanical fully coupled and non-coupled way. The full coupling has no advantages on the accuracy of the solution but increase the costs (computation time). Both simulations should run in batch mode. Hybrid implicit/explicit simulations cannot achieve the required accuracy, because the explicit mechanical part is not able to simulate the distortion (thermal spring back). Accelerating the explicit simulations (time-scaling), lead to significant numerical errors and cause early termination of the solver.

A rough mesh with a minor time-step ($\Delta t$ = 0.250 s) shows equivalent results (deviation of about 5%) as the fine mesh with a big time-step ($\Delta t$ = 0.50 s) and requires a computation time of 686 min instead of 2467 min. Bigger time-steps lead to more iterations and increase in the computation time. Further time reductions can be achieved by using non-coupled but simultaneous solver techniques. The effect of ghost material properties on the simulation results were discussed in 3.3. Low Young's modulus (100 N/mm²) show nearly no influence on the welding process, but introduces numerical instabilities. Therefore, for small mesh-sizes and small step-sizes the Young's modulus should be increased, even when it introduces unwanted stresses.

In future work, the influence of the thermal cycles on the microstructure will be investigated.

ACKNOWLEDGMENT

*The authors would like to thank the Deutscher Akademischer Austauschdienst e.V. for supporting this research (Funding number DAAD-HEC-UESTP (50015636)).*

REFERENCE

[1] WILLIAMS S.W., MARTINA F., ADDISON A.C., DING J., PARDAL G., COLEGROVE P., 2015, *Wire + Arc Additive Manufacturing*, Materials Science and Technology, 32/7, 641–647.
[2] LIU G.R., LIU M., 2009, *Smoothed particle hydrodynamics*: *A meshfree particle method*, World Scientific Publishing Company, New Jersey, https://doi.org/10.1142/5340.
[3] ZHANG L., MICHALERIS P., 2004, *Investigation of Lagrangian and Eulerian finite element methods for modeling the laser forming process*, Finite Elements in Analysis and Design, 40/4, 383–405.
[4] DONEA J., HUERTA A., PONTHOT J.-Ph., RODRIGUEZ-FERRAN A., 2004, *Arbitrary Lagrangian–Eulerian Methods*, Chapter 14, Encyclopedia of Computational Mechanics, Edited by E. Stein, R. de Borst and Thomas J.R. Hughes, Volume 1, Fundamentals, John Wiley & Sons, Ltd., 413–437, ISBN: 0-470-84699-2.
[5] KUCHARIK M., LISKA R., VACHAL P., SHASHKOV M., 2006, *Arbitrary Lagrangian-Eulerian (ALE) methods in compressible fluid dynamics*, Programs and Algorithms of Numerical Mathematics, 13, 178–183.
[6] FERZIGER J.H., PERIĆ M., 2002, *Computational Methods for Fluid Dynamics*, Springer-Verlag Berlin Heidelberg NewYork, ISBN 3-540-42074-6.
[7] RAN W., CHENG W., QIN F., LUO X., 2011, *GPU accelerated CESE method for 1D shock tube problems*, Journal of Computational Physics, 230/24, 8797–8812.
[8] MISHRA B.K., RAJAMANI RAJ K., 1992, *The discrete element method for the simulation of ball mills*, Appl. Math. Modelling, 16/11, 598–604.
[9] LIANG D., JIAN W., SHAO S., CHEN R., YANG K., 2017, *Incompressible SPH simulation of solitary wave interaction with movable seawalls*, Journal of Fluids and Structures, 69, 72–88.
[10] BELYTSCHKO T., LU Y.Y., GU L., 1994, *Element-free Galerkin methods*, Int. J. for Numerical Methods in Engineering, 37/2, 229–256.
[11] BELLET M., HAMIDE M., 2013, *Direct modeling of material deposit and identification of energy transfer in gas metal arc welding*, Int. J. of Num. Meth. for HFF, 23/8, 1340–1355.
[12] CHENG G.C., VENKATACHARI B.S., CHANG C.L., CHANG S.C., 2011, *Comparative study of different numerical approaches in space-time CESE framework for high-fidelity flow simulations*, Computers & Fluids, 45/1, 47–54.
[13] WILLIAMS P.T., BAKER A.J., 1996, *Incompressible Computational Fluid Dynamics and the Continuity Constraint Method for the Three-Dimensional Navier-Stokes Equations*, Numerical Heat Transfer, Part B, Fundamentals, 29/2, 137–273.
[14] HAJIAZIZI M., BASTAN P., 2014, *The elastoplastic analysis of a tunnel using the EFG method*, *A comparison of the EFGM with FEM and FDM*, Applied Mathematics and Computation, 234, 82–113.
[15] ALSHAER A.W., ROGERS B.D., LI L., 2017, *Smoothed Particle Hydrodynamics (SPH) modelling of transient heat transfer in pulsed laser ablation of Al and associated free-surface problems*, Computational Materials Science, 127, 161–179.
[16] PENG C., XU G., WU W., YU H.S., WANG C., 2017, *Multiphase SPH modeling of free surface flow in porous media with variable porosity*, Computers and Geotechnics, 81, 239–248.
[17] NATSUI S., NASHIMOTO R., TAKAI H., KUMAGAI T., KIKUCHI T., SUZUKI R.O., 2016, *SPH simulations of the behavior of the interface between two immiscible liquid stirred by the movement of a gas bubble*, Chemical Engineering Science, 141, 342–355.
[18] RAHUL B., 2012, *Using DEM to Solve Bulk Material Handling Problems*, American Institute of Chemical Engineers (AIChE), 54–58.

[19] ABBASFARD H., EVANS G., MORENO-ATANASIO R., 2016, *Effect of van der Waals force cut-off distance on adhesive collision parameters in DEM simulation*, Powder Technology, 299, 9–18.
[20] HAREWOOD F.J., MCHUGH P.E., 2007, *Comparison of the implicit and explicit finite element methods using crystal plasticity*, Computational Materials Science, 39/2, 481–494.
[21] SUN J.S., LEE K.H., LEE H.P., 2000, *Comparison of implicit and explicit finite element methods for dynamic problems*, Journal of Materials Processing Technology, 105/1–2, 110–118.
[22] HU X., WAGONER R.H., DAEHN G.S., GHOSH S., 1994, *Comparison of explicit and implicit finite element methods in the quasistatic simulation of uniaxial tension*, Communications in Numerical Method in Engineering, 10/12, 993–1003.
[23] CHOI H.H., HWANG S.M., KANG Y.H., KIM J., KANG B.S., 2002, *Comparison of Implicit and Explicit Finite-Element Methods for the Hydroforming Process of an Automobile Lower Arm*, The International Journal of Advanced Manufacturing Technology, 20/6, 407–413.
[24] KORIC S., HIBBELER L.C.,THOMAS B.G., 2009, *Explicit coupled thermo-mechanical finite element model of steel solidification*, Int. J. for Numerical Methods in Engineering, 78/1, 1–31.
[25] YANG D.Y., JUNG D.W., SONG I.S., YOO D.J., LEE J. H., 1995, *Comparative investigation into implicit, explicit, and iterative implicit/explicit schemes for the simulation of sheet-metal forming processes.* Journal of Materials Processing Technology, 50/1–4, 39–53.
[26] LINDGREN, L.E., 2006, *Numerical modelling of welding*, Computer Methods in Applied Mechanics and Engineering, 195/48–49, 6710–6736.
[27] MURAKAWA H., MA N., HUANG H., 2015, *Iterative substructure method employing concept of inherent strain for large-scale welding problems*, Weld World, 59/1, 53–63.
[28] MA N., NARASAKI K., 2018, *Simulation of welding thermal conduction and thermal stress using hybrid method of accelerated explicit and implicit FEM*, J. Phys. Conf. Ser. 1063, 12073.
[29] ISRAR R., BUHL J., ELZE L., BAMBACH M., 2018, *Simulation of different path strategies for wire-arc additive manufacturing with Lagrangian finite element methods*, LS-DYNA Forum 2018, Bamberg Germany.
[30] LINDSTRÖM P., 2015. *Improved CWM platform for modelling welding procedures and their effects on structural behaviour*, PhD Thesis, University West, Trollhättan.
[31] NADIMI S., KHOUSHEHMEHR R.J., ROHANI B., MOSTAFAPOUR A., 2008, *Investigation and Analysis of Weld Induced Residual Stresses in Two Dissimilar Pipes by Finite Element Modeling*, J. of Applied Sciences, 8/6, 1014–1020.
[32] MONTEVECCHI F., VENTURINI G., SCIPPA A., CAMPATELLI G., 2016, *Finite Element Modelling of Wire-arc-additive-manufacturing Process*, Procedia CIRP, 55, 109–114.
[33] CHIUMENTI M., CERVERA M., SALMI A., AGELET DE SARACIBAR C., DIALAMI N., MATSUI K., 2010, *Finite element modeling of multi-pass welding and shaped metal deposition processes*, Computer Methods in Applied Mechanics and Engineering, 199/37–40, 2343–2359.
[34] ERHART T., Ed., 2011. *Review of Solid Element Formulation in LS-DYNA, Properties, Limits, Advantages, Disadvantages*, DYNAmore, Stuttgart.